Research Article

ADVANCED PHOTONICS

Nonlinear optical trapping effect with reverse saturable absorption

Zheng Zhu,[a,b,c,†] Yuquan Zhang,[a,*,†] Shuoshuo Zhang,[a] Aurèle J. L. Adam,[c] Changjun Min,[a] Hendrik Paul Urbach,[c,*] and Xiaocong Yuan[b,a,*]

[a]Shenzhen University, Institute of Microscale Optoelectronics and State Key Laboratory of Radio Frequency Heterogeneous Integration, Nanophotonics Research Center, Shenzhen, China

[b]Research Institute of Intelligent Sensing, Research Center for Humanoid Sensing, Zhejiang Lab, Hangzhou, China

[c]Delft University of Technology, Optics Research Group, Delft, The Netherlands

Abstract. Nonlinear responses of nanoparticles induce enlightening phenomena in optical tweezers. With the gradual increase in optical intensity, effects from saturable absorption (SA) and reverse SA (RSA) arise in sequence and thereby modulate the nonlinear properties of materials. In current nonlinear optical traps, however, the underlying physical mechanism is mainly confined within the SA regime because threshold values required to excite the RSA regime are extremely high. Herein, we demonstrate, both in theory and experiment, nonlinear optical tweezing within the RSA regime, proving that a fascinating composite trapping state is achievable at ultrahigh intensities through an optical force reversal induced through nonlinear absorption. Integrated results help in perfecting the nonlinear optical trapping system, thereby providing beneficial guidance for wider applications of nonlinear optics.

Keywords: nonlinear optical tweezers; optical force; reverse saturable absorption.

Received Feb. 4, 2023; revised manuscript received Jun. 27, 2023; accepted for publication Jul. 3, 2023; published online Aug. 1, 2023.

[DOI: 10.1117/1.AP.5.4.046006]

1 Introduction

Optical tweezers can exert piconewton forces on small objects to manipulate their motion in a liquid surrounding medium.[1,2] A stable optical trapping is based on the balance between scattering and gradient forces.[3,4] This convenient and intuitive principle works in establishing and describing the normal configurations of optical tweezers and has been widely employed in physical,[5,6] biological,[7] and chemical research.[8] Currently, the nonlinear effects in optical trapping unveil new possibilities and opportunities previously unprecedented. Nonlinear interactions occur between the nano-objects and ultrahigh-peak pulses, from which comprehensive and novel phenomena emerge with the subverted balance of the original optical force.[9–11] For example, gold nanoparticles trapped in a linearly polarized beam present an unprecedented result that one trap site was split into two.[9] The adjustable distance between two spaced trapping positions can reach beyond the diffraction limit of the focus field without any other complex optical instruments. The nonlinear response of the nano-object gives rise to the significant impact on its physical parameters and properties,[12–15] thereby providing an additional regulatory dimension to the trapped objects.

However, the peak intensity of the trapping pulse employed in current nonlinear optical tweezers resides at relatively low excitation levels.[10] In these circumstances, the nonlinear interaction lies within the saturable absorption (SA) regime in which the coefficient of absorption for the nano-object decreases towards a saturation value.[16,17] For SA, the electrons of the absorptive medium are stimulated from the ground state to an excited state and leads to ground-state bleaching, in which the medium no longer is able to absorb photons and the transmittance of the material increases. In this process, the nonlinear absorption destroys the balance of the original forces and thus creates a split optical trap.[9–11] When the intensity of the pulse continues to increase through the accompanying transitions between energy levels of the excited states, the coefficient of absorption for the medium increases with higher excitation levels in a process

*Address all correspondence to Yuquan Zhang, yqzhang@szu.edu.cn; Hendrik Paul Urbach, h.p.urbach@tudelft.nl; Xiaocong Yuan, xcyuan@zhejianglab.com

†These authors contributed equally to this work.

known as reverse SA (RSA).[18–24] Within this RSA regime, the equilibration of forces is further modulated and extends the range of the nonlinear optical tweezing. However, the research on this topic at present is still comparatively immature.

In this work, we demonstrate a nonlinear optical trapping system operating within the RSA regime and develop a completed conceptually explicit mechanism of nonlinear optical tweezing. With this system, a nonlinear optical trapping of gold nanoparticles is achievable, demonstrated both in theory and experiment, by employing a femtosecond laser pulse of circularly polarized light. When the peak intensity of the pulse surpasses the threshold to excite the deep RSA regime, a remarkably composite state in the optical trap appears, comprising a circumgyration state of one particle encircling a central stationary state of another. The experimental results of the phenomena match well with theoretical predictions. The results help to perfect the nonlinear optical tweezer system for trap loading. Using universal materials with nonlinear responses, which make a substantial contribution, the nonlinear optical trapping mechanism that we reveal may be important in developing new modalities of manipulating nanoscale objects by choosing prescribed light intensities appropriate for a nonlinear response.

2 Theory

Gold nanoparticles possess evident nonlinear optical properties and feature a complex refractive index that depends on the applied field intensity in the presence of Kerr-type nonlinearity.[25–27] Numerous works have indicated that gold nanoparticles exhibit distinct responses in the SA and RSA regimes.[17–22] Physically, the rate of change in the coefficient of nonlinear absorption for a gold nanoparticle remains negative during SA, but switches to being positive within the RSA regime. This reversal of sign produces significant changes in physical properties. The dependence on intensity of the coefficient of nonlinear absorption κ for gold nanoparticle is calculated from Ref. 26,

$$\kappa = \frac{\lambda}{4\pi}\left(\frac{a_0}{1 + I/I_s} + \beta I\right), \tag{1}$$

where I_s denotes the saturable optical intensity, β the coefficient of two-photon absorption, and a_0 the coefficient of linear absorption for a gold nanoparticle. The complex refractive index of the gold nanoparticle can be obtained from $n_p = n_0 + n_2 I + \mathrm{i}\kappa$; where n_0 denotes the real part of the linear refractive index and n_2 the real part of the nonlinear refractive index. It is known that the real part of the nonlinear refractive index is much smaller than the imaginary part. Thus, as an approximation, we set the real part equal to zero.[28] As the complex n_p depends strongly on the coefficient of nonlinear absorption κ, the actual polarizability of the gold dipole varies with field intensity. In simulations of gold nanoparticles, we set $I_s = 55 \times 10^{14}$ W/m^2 (see Supplementary Note IV in the Supplementary Material), $n_0 = 0.41661 + 5.2347\mathrm{i}$, and $a_0 = 7.8311 \times 10^7$ m^{-1}.[29]

Figure 1 attributes the nonlinear response of gold nanoparticles to an increase in the field intensity of a femtosecond pulse. To stimulate the SA and RSA effects, a focused circularly polarized femtosecond pulsed laser is applied as an excitation source. The focused field is determined by Debye vectorial diffraction theory (see Supplementary Note II in the Supplementary Material).[30] Here, consistent with the experimental conditions, the NA of the objective lens is set to 0.65. Values for the characteristic parameters of the pulsed laser are pulse width $\tau = 100$ fs, repetition frequency $\nu = 80$ MHz, and central wavelength $\lambda = 840$ nm.

Referring to the gold nanoparticles used in this work, Fig. 1(a) shows the distribution of coefficient of nonlinear absorption κ as a function of two-photon absorption coefficient and incident peak intensity. The white line marks the boundary of the SA and RSA regimes. By increasing the peak intensity from 0 to 14 TW/cm^2, the SA and RSA effects are clearly evoked in sequence, and the coefficient of two-photon absorption β is a crucial parameter in determining the transition threshold. From experimental measurements, we set $\beta = 29$ cm/GW.[18] Figure 1(b) shows a plot of the change in κ for a gold nanoparticle as a function of peak intensity under the specific condition. During SA, the coefficient of absorption decreases with a relatively low excitation power but starts increasing when entering the RSA regime, with the power overcoming the threshold value of 3.32 TW/cm^2.

Figure 2(a) plots the relation between incident average power (P_{ave}) and peak intensity of the focusing field (I_{peak}); an average incident power range of 0 to 2.0 W is able to excite both SA and

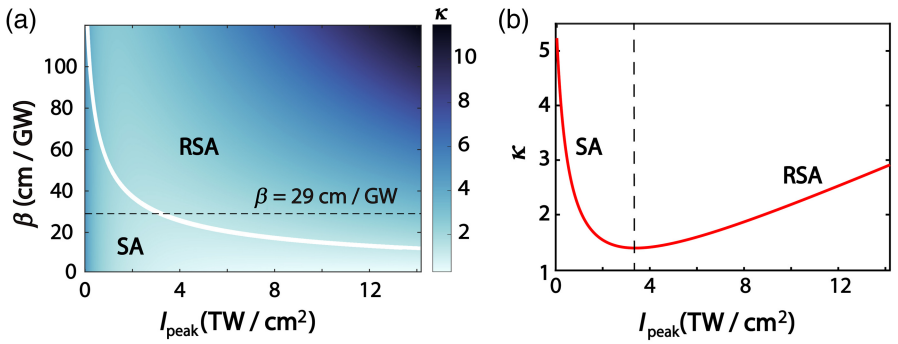

Fig. 1 Nonlinear absorption of gold nanoparticles. (a) Coefficient of nonlinear absorption κ against the two-photon absorption coefficient β and the peak intensity of excitation field I_{peak}. The white solid line marks the boundary between the SA and RSA regimes. (b) Change in the coefficient of nonlinear absorption κ as a function of I_{peak} when $\beta = 29$ cm/GW. The black dashed line in panel (b) is the dividing line between the SA and RSA regimes. The diameter of the gold nanoparticle is 60 nm; the medium in which the particle was immersed is water.

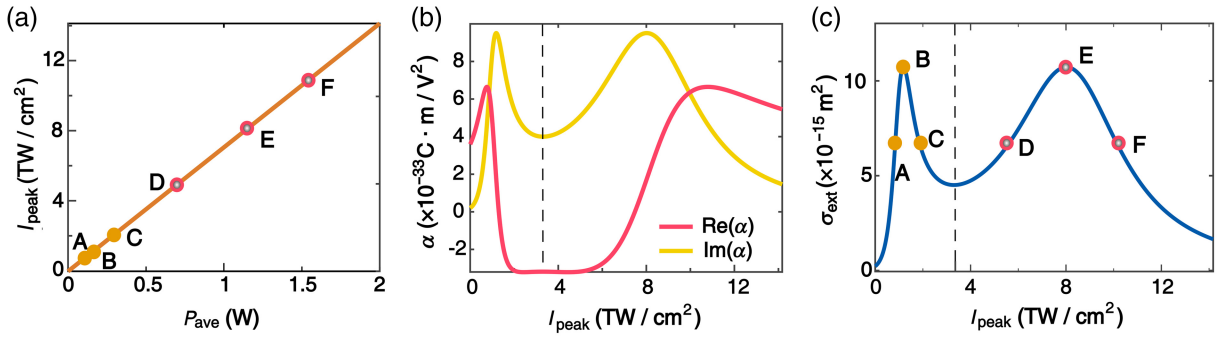

Fig. 2 Nonlinear polarizability and extinction cross section of gold nanoparticles. (a) Peak intensity of the focused excitation field as a function of averaged incident power P_{ave} ranging from 0 to 2.0 W. (b) Real and imaginary parts of the nonlinear polarizability α change with increasing excitation intensity. (c) Extinction cross section σ_{ext} varies with excitation intensity; a maximum value occurs for SA and RSA. Dashed lines in panels (b) and (c) mark threshold values between SA and RSA.

RSA effects. The sign reversal in the rate of change for the coefficient of nonlinear absorption in the SA and RSA regimes produces significant influences in basic optical properties. These changes play vital roles in the nonlinear optical trapping process, reflected most apparently through the polarizability α and extinction cross section σ_{ext}. Here, the polarizability α of a gold nanoparticle under the dipole approximation is given as[31,32]

$$\alpha = \frac{\alpha_0}{1 - i\alpha_0 k^3/(6\pi\varepsilon)}, \quad \alpha_0 = 4\pi\varepsilon r^3 \frac{n_p^2 - n_h^2}{n_p^2 + 2n_h^2}, \tag{2}$$

where k denotes the wavenumber of the incident optical field in the host medium, ε the permittivity of the host medium, r the particle radius, and n_h the refractive index of the host medium; the extinction cross section of a single particle σ_{ext} is then obtained from $\sigma_{ext} = k\,\mathrm{Im}(\alpha)/\varepsilon$.[32]

Figures 2(b) and 2(c) plot the real polarizability of the gold nanoparticle, which determines the gradient force, and the extinction cross section, which depends on the imaginary part of α and contributes to the scattering force. With increasing incident power, two peaks are apparent for both parameters; the dashed lines indicate the switching threshold between the SA and RSA regimes. Consequently, by varying the incident power to modulate the final trapping forces, a fully well-equipped universal nonlinear optical tweezers system is constructed. It is noteworthy that the optical resonance effect (ORE) can affect optical forces exerted on the nanoparticle.[33,34] At the resonance wavelength of the gold nanoparticle, the imaginary part of polarizability $\mathrm{Im}(\alpha)$ is amplified, indicating an increased scattering force. On the other hand, the real parts of polarizability $\mathrm{Re}(\alpha)$ and the gradient force are close to their minimum values.[35] For this scenario, the gold nanoparticle suffers a large scattering force and is difficult to trap. Therefore, we use the near-infrared pulsed laser as a light source to keep away from the resonant condition.

The optical force depends on the polarizability of the dipole and the surrounding electric field. The equation for the time-averaged forces is based on the dipole approximation theory.[36] For a femtosecond pulsed optical field, the force is written as (see Supplementary Note III in the Supplementary Material)

$$\langle F \rangle = \tau\nu \left\{ \frac{1}{4}\,\mathrm{Re}(\alpha)\nabla|E_0|^2 + \frac{\sigma_{ext} c\varepsilon}{2n_h\omega_0}\,\mathrm{Im}[E_0^* \cdot (\nabla)E_0] \right\}, \tag{3}$$

where E_0 denotes the peak electronic field at the particle position, c the light speed in a vacuum, and ω_0 the central frequency of the pulse.

3 Results and Discussion

Nonlinear optical tweezers operating within the SA regime have been previously described in detail;[9–11] some details are presented in the Supplementary Note V in the Supplementary Material. In response to the SA effect, a bulging potential energy barrier surfaces within a circular energy ravine (Fig. S4 in the Supplementary Material), and a circumgyration has been experimentally demonstrated along an annular energy flow (Fig. S4 in the Supplementary Material). Here, we focus on the trapping effect and the switching process within the RSA regime. Figures 3(a) and 3(b) show schematics of the nonlinear optical trap formed by a femtosecond circularly polarized laser pulse operating within the early and deep RSA regimes, respectively. In the former, the potential well is distributed similar to that within the SA regime; more interestingly, for the latter, a sharp sink appears at the center of the energy barrier surrounded by the still-maintained potential energy ravine. Consequently, a gold nanoparticle is constrained stably at the center while others are constrained in the outer ring and undergo circumgyration.

To confirm this assertion, various experiments were conducted; the experimental setup implemented is depicted in schematics given in Fig. S1 in the Supplementary Material (Supplementary Note I in the Supplementary Material). Incident powers of 1.15 and 1.54 W were employed to excite the early and deep RSA responses. Figure 3(c) plots the trajectories of a trapped gold nanoparticle undergoing circumgyration in the potential well. Similarly, Fig. 3(d) presents the superimposed results of two trapped gold nanoparticles; red dots indicate the trajectory of a stably trapped nanoparticle at the center, whereas yellow dots mark that of a circumgyrating nanoparticle.

To understand the nonlinear physical mechanism more thoroughly, the evolution of the optical force and potential well within the RSA regime is elaborated. Typical values, labeled in Figs. 2(a) and 2(c), were selected for elucidation; points A

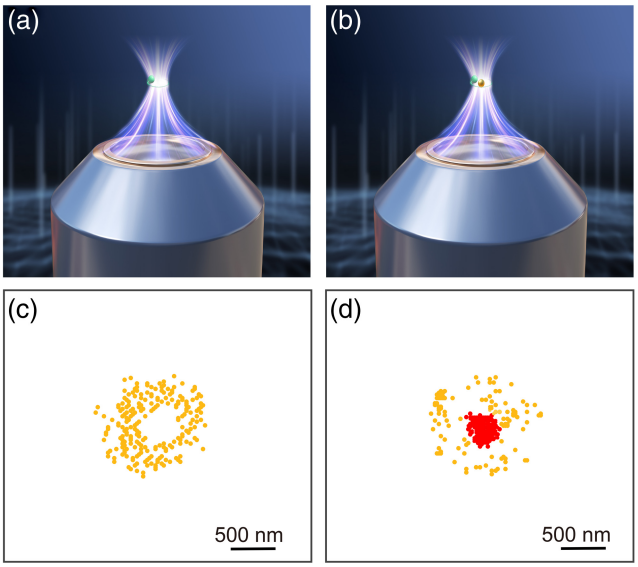

Fig. 3 Nonlinear optical tweezers within the RSA regime. (a) and (b) Schematics of the trapping states of gold nanoparticles within the early and deep RSA regimes. (c) and (d) Recorded particle trajectories obtained from experiments operating in the early and deep RSA regimes, respectively.

to C are situated in the SA regime, whereas points D to F lie in the RSA regime. As to the switching process of the nonlinear optical trapping effect within the RSA regime, the nonlinear optical forces and trapping potential wells in the focal plane under the selected incident powers—corresponding to points D to F—were plotted [Figs. 4(a)–4(f)]. Combined with vectorial diffraction theory, the direction and distribution of the optical force were subsequently calculated based on the dipolar approximation method.

When the nonlinear effect begins to gain ground within the RSA regime, the extinction cross section displays a nonmonotonic change with increasing incident power. With this change, the original force equilibrium is perturbed to form a "neo-potential well." For the three selected incident average power values in the RSA regime [D, E, and F in Fig. 2(c)], the optical force and potential well were plotted [Figs. 4(a)–4(c) and 4(d)–4(f), respectively]. Both the magnitude and region of the reversed optical force are enlarged. The detailed description of the force variation tendency in the central region from point D to F is included in Supplementary Note VI in the Supplementary Material. By increasing the incident power, the size of the ring-shaped nonlinear potential well slightly expands in the early RSA regime [Figs. 4(a) and 4(b)]. Here, the trapping potential has been normalized using k_BT, where k_B denotes the Boltzmann constant and T ($T = 300$ K) the absolute temperature of the environment. At the incident average power of 0.7 W (point D in Fig. 2), a potential barrier with a positive peak value of $20k_BT$ is achieved to sweep the particles in this area away; meanwhile, a ring-shaped potential well having a negative extreme value of $-19k_BT$ remains almost unchanged from that found at the boundary of the SA regime [Fig. S4(f) in the Supplementary Material]. At the peak point of the extinction cross section in the RSA regime, i.e., point E with an average power of 1.15 W, the optical force is close to zero at the focal center point, signifying that a subsequent reversal emerges [Figs. 4(b) and 4(e)]. In this circumstance, the central potential barrier flattens out, and a maximum positive potential barrier of $44k_BT$ forms.

With a further increase in the average power, an optical force with a sign reversal arises from the central point and expands gradually. Simultaneously, under this reversed optical force, the center of the convex positive potential barrier subsides, producing a "volcano-like" profile in the potential [Figs. 4(c) and 4(f)]. For the relatively high power of 1.54 W at point F, the original ring-shape potential depth remains nearly constant at $-19k_BT$. The centrally generated neo-potential well possesses a relatively deeper value of $-33k_BT$ compared with the surroundings. Although the absolute minimum value of the central subsidence is positive, it is still encircled by a more powerful annular barrier. Ultimately, a strongly stable optical trap appears at the center, surrounded by a trap-functioning ravine-like potential.

To verify the physical phenomenon of nonlinear optical trapping within the RSA regime, two specific average powers (1.15 and 1.54 W) were selected for experimental demonstration. As there exists an annular energy flow in the longitudinal component of the focused field, the trapped nanoparticles are driven to rotate along the circular ravine. Figures 4(g) and 4(h) present successive frames of a video (Videos 1 and 2), from which trajectories were plotted [Figs. 3(c) and 3(d)]. In the early RSA regime, the optical force and trapping potential well retain a similarity to that of the SA regime (Fig. S4 in the Supplementary Material). A circumgyration also develops at $P_{ave} = 1.15$ W. For the experiments at $P_{ave} = 1.54$ W, in addition to a circumgyrating nanoparticle, another particle is trapped at the center point inside the path of circumgyration. The bright flare at the center verifies the high stability of the central trapped nanoparticle, whereas the fall in brightness in the outer ring results from the particle being in a state of circumgyration of high speed. We conclude that circumgyration originally arising in the SA regime holds steady, and a second trap is formed through the deep RSA effect. Considering the small number of trapped nanoparticles and their size being significantly smaller than the incident wavelength, the optical binding effect[37] can be safely disregarded. After careful comparison with Ref. 10, the rotation rate of circumgyration is estimated as 200 to −300 Hz within the RSA regime (see Supplementary Note VII in the Supplementary Material).

The optical force originates from the physical properties of the trapped objects and its interactions with the optical field. The consensus is that stable optical trapping is achieved through the balance of optical forces. The nonlinear response of the gold material is excited in an ultrahigh electric field; however, it disturbs the established balance. Its transmittance increases as a consequence of SA and diminishes under RSA. With an incident femtosecond pulse of circularly polarized light, the optical forces exerted thereby on a gold nanoparticle reduce and reverse in the SA regime. The potential profile changes from concave to convex at the central position. Consequently, at relatively low intensities in the nonlinear optical tweezers, a ring-shaped potential well can be formed, and nanoparticles can be driven to circumgyrate along the orbital energy flux.

As input power increases, nonlinear RSA comes into effect, and the convex energy barrier strengthens gradually. When the incident intensity reaches a specific threshold value, the magnitude of the optical forces becomes smaller and another reversal in direction of the optical forces appears at the center. From a

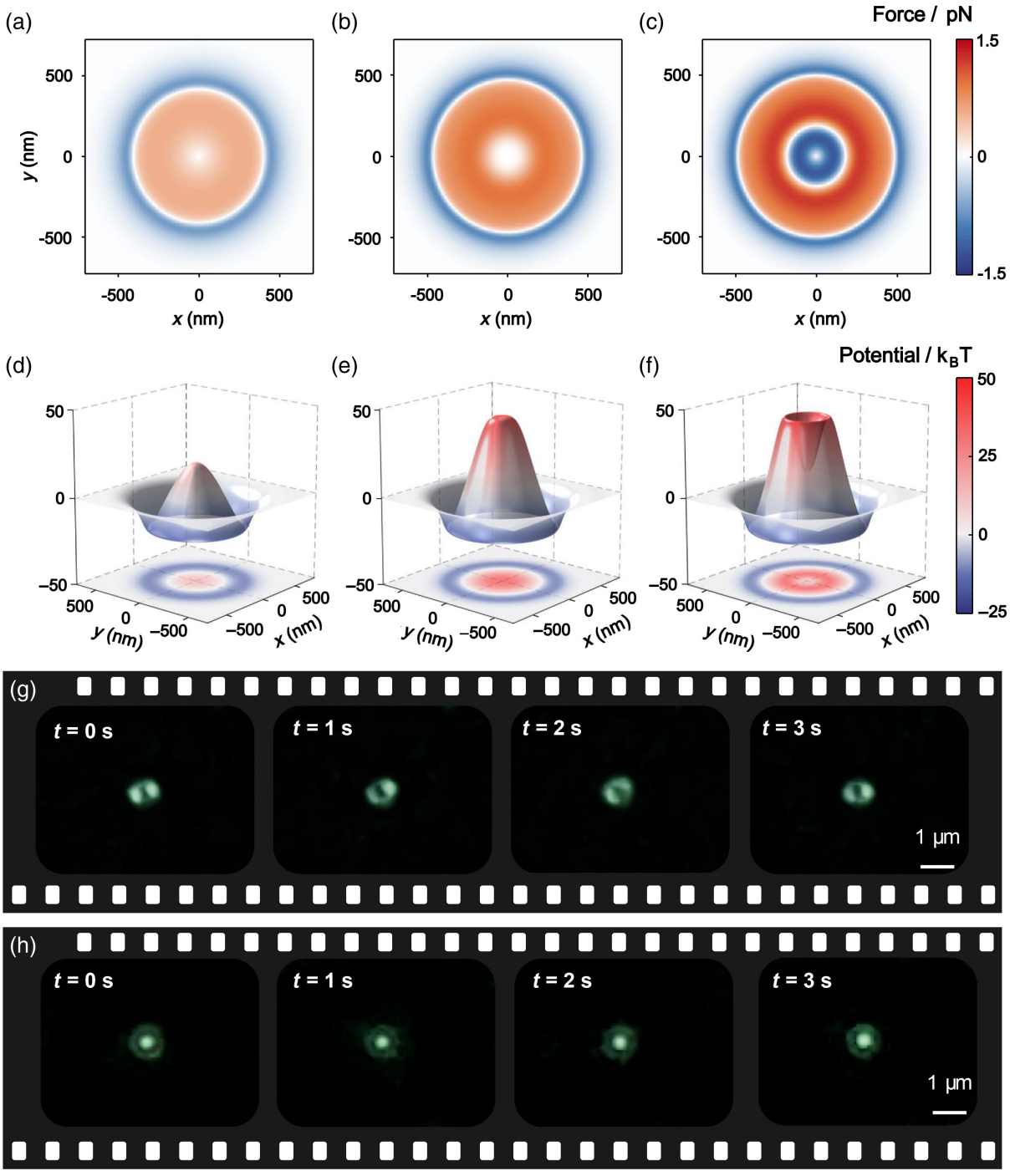

Fig. 4 Switching of the nonlinear optical tweezers from the early to the deep RSA regime. (a)–(c) Radial optical force and (d)–(f) trapping potential distributions in the focal plane acting on the gold nanoparticle, for averaged incident power $P_{ave} = 0.7$ W, 1.15 W, and 1.54 W, corresponding to respective points D, E, and F labeled in Fig. 2. (g) and (h) Experimental screenshots of gold nanoparticles trapped under incident powers of 1.15 and 1.54 W, respectively. Because of the distinctive trapping potential formed within the deep RSA regime, a gold nanoparticle is constrained stably at the center, while another performs an outer circumgyration (Video 1, MP4, 888 KB [URL: https://doi.org/10.1117/1.AP.5.4.046006.s1]; Video 2, MP4, 200 KB [URL: https://doi.org/10.1117/1.AP.5.4.046006.s2]).

potential energy perspective, a neo-subsidence appears at the original convex vertex within a larger excitation, indicating that an additional particle is trapped at the center, encircled by the original circumgyrating nanoparticle(s). Hereto, a completed nonlinear optical trapping mechanism is established in theory and demonstrated in experiments. It is noteworthy that the usage of femtosecond-pulsed illumination can lead to a sharp and transient increase in temperature of the nanoparticle. This effect can confine the heat within the close vicinity of the nanoparticle, which prevents extended heating of the surrounding environment to destabilize the stable optical trapping (see Supplementary Note VIII in the Supplementary Material).

In the nonlinear regime, it is possible to achieve subdiffraction-limit controllable rotation of gold nanoparticles. A quantitative analysis of the mechanism governing the nonlinear optical trapping effect improves our understanding of the physics of light–matter interactions. Implementing nonlinear composite optical manipulation phenomena now becomes possible, with the potential for an expansion in applications. For example, these optical tweezers can be utilized as optically driven sensors and machines for microfluidic environments.[38–40] Furthermore, the ability to control the speed, radius, and direction of rotation is of great value in metrology.[41,42]

4 Conclusion

Using a circular polarization femtosecond beam, we performed intensive research on the evolution of nonlinear properties and responses of gold nanoparticles, as well as the nonlinear optical forces that accompany the process. Within the deep RSA regime, a composite trapping state, i.e., a state in which an additional static trap encircled by the original circumgyration appears at the very center, is demonstrated. The results from experiments match well with those from theory. The demonstration proves that the switching of trap states stems from a reversal of the optical forces, which is induced through the reversal in sign of the rate of change in the coefficient of nonlinear absorption. The results fill gaps in knowledge of the existing nonlinear optical tweezing, and help in perfecting a relatively complete physical system. Our understanding of the mechanism underscoring nonlinear optical trapping is improved, thus paving the way for a broader study of nonlinear metallic materials. Furthermore, the novel nonlinear optical trapping effect has the potential to synergize with diverse structured light beams and other nonlinear materials, including quantum dots and nonlinear nanocrystals. More novel trap phenomena binding with other nanotechnologies are expected to be discovered for the extension of the physical significance of nonlinear optical trapping, as well as being conducive to the further developments in practical applications.

Code, Data, and Materials Availability

Data underlying the results presented in this paper may be obtained from the authors upon reasonable request.

Acknowledgments

This work was supported by the Guangdong Major Project of Basic and Applied Basic Research (Grant No. 2020B0301030009); the National Natural Science Foundation of China (Grant Nos. 61975128, 61935013, and 62175157); the Shenzhen Science and Technology Program (Grant Nos. JCYJ20210324120403011 and RCJC20210609103232046); the Natural Science Foundation of Guangdong Province (Grant No. 2019TQ05X750); the Key Research Project of Zhejiang Lab (Grant No. 2022MG0AC05); and thre Shenzhen Peacock Plan (Grant No. KQTD20170330110444030). The authors declare no competing financial interests.

References

1. A. Ashkin, "Acceleration and trapping of particles by radiation pressure," *Phys. Rev. Lett.* **24**(4), 156–159 (1970).
2. A. Ashkin, J. Dziedzic, and T. Yamane, "Optical trapping and manipulation of single cells using infrared laser beams," *Nature* **330**(6150), 769–771 (1987).
3. A. Ashkin et al., "Observation of a single-beam gradient force optical trap for dielectric particles," *Opt. Lett.* **11**(5), 288–290 (1986).
4. K. C. Neuman and S. M. Block, "Optical trapping," *Rev. Sci. Instrum.* **75**(9), 2787–2809 (2004).
5. Y. Yang et al., "Optical trapping with structured light: a review," *Adv. Photonics* **3**, 034001 (2021).
6. Y. Yu et al., "Roadmap for single-molecule surface-enhanced Raman spectroscopy," *Adv. Photonics* **2**, 014002 (2020).
7. A. D. Mehta et al., "Single-molecule biomechanics with optical methods," *Science* **283**(5408), 1689–1695 (1999).
8. H. Misawa, N. Kitamura, and H. Masuhara, "Laser manipulation and ablation of a single microcapsule in water," *J. Am. Chem. Soc.* **113**(21), 7859–7863 (1991).
9. Y. Q. Jiang, T. Narushima, and H. Okamoto, "Nonlinear optical effects in trapping nanoparticles with femtosecond pulses," *Nat. Phys.* **6**(12), 1005–1009 (2010).
10. Y. Q. Qin et al., "Nonlinearity-induced nanoparticle circumgyration at sub-diffraction scale," *Nat. Commun.* **12**, 3722 (2021).
11. Y. Q. Zhang et al., "Nonlinearity-induced multiplexed optical trapping and manipulation with femtosecond vector beams," *Nano Lett.* **18**(9), 5538–5543 (2018).
12. B. Sain, C. Meier, and T. Zentgraf, "Nonlinear optics in all-dielectric nanoantennas and metasurfaces: a review," *Adv. Photonics* **1**, 024002 (2019).
13. X. Hao and C. Kuang, "Towards extremely high-order optical nonlinearity at the nanoscale," *Adv. Photonics* **4**, 020501 (2022).
14. M. Kauranen and A. V. Zayats, "Nonlinear plasmonics," *Nat. Photonics* **6**(11), 737–748 (2012).
15. A. E. Minovich et al., "Functional and nonlinear optical metasurfaces," *Laser Photonics Rev.* **9**(2), 195–213 (2015).
16. G. Wang, A. A. Baker-Murray, and W. J. Blau, "Saturable absorption in 2D nanomaterials and related photonic devices," *Laser Photonics Rev.* **13**(7), 1800282 (2019).
17. L. D. Boni et al., "Optical saturable absorption in gold nanoparticles," *Plasmonics* **3**, 171–176 (2008).
18. K. Wang et al., "Size-related third-order optical nonlinearities of Au nanoparticle arrays," *Opt. Express* **18**(13), 13874–13879 (2010).
19. Y. Gao et al., "Saturable absorption and reverse saturable absorption in platinum nanoparticles," *Opt. Commun.* **251**, 429–433 (2005).
20. H. I. Elim et al., "Observation of saturable and reverse-saturable absorption at longitudinal surface plasmon resonance in gold nanorods," *Appl. Phys. Lett.* **88**(8), 083107 (2006).
21. U. Gurudas et al., "Saturable and reverse saturable absorption in silver nanodots at 532 nm using picosecond laser pulses," *J. Appl. Phys.* **104**(7), 073107 (2008).
22. K. Wang et al., "Intensity-dependent reversal of nonlinearity sign in a gold nanoparticle array," *Opt. Lett.* **35**(10), 1560–1562 (2010).
23. L. W. Tutt and T. F. Boggess, "A review of optical limiting mechanisms and devices using organics, fullerenes, semiconductors and other materials," *Prog. Quant. Electron.* **17**(4), 299–338 (1993)

24. X. Liu, Q. Guo, and J. Qiu, "Emerging low-dimensional materials for nonlinear optics and ultrafast photonics," *Adv. Mater.* **29**(14), 1605886 (2017).
25. X. Zhang et al., "Tunable ultrafast optical switching via waveguided gold nanowires," *Adv. Mater.* **20**(23), 4455–4459 (2008).
26. Y. H. Lee et al., "Nonlinear optical switching behavior of Au nanocubes and nano-octahedra investigated by femtosecond Z-scan measurements," *Appl. Phys. Lett.* **95**(2), 023105 (2009).
27. R. West, Y. Wang, and T. Goodson, "Nonlinear absorption properties in novel gold nanostructured topologies," *J. Phys. Chem. B* **107**(15), 3419–3426 (2003)
28. R. W. Boyd, Z. Shi, and I. D. Leon, "The third-order nonlinear optical susceptibility of gold," *Opt. Commun.* **326**, 74–79 (2014).
29. H. J. Hagemann, W. Gudat, and C. Kunz, "Optical constants from the far infrared to the X-ray region: Mg, Al, Cu, Ag, Au, Bi, C, and Al_2O_3," *J. Opt. Soc. Am.* **65**(6), 742–744 (1975).
30. B. Richards and E. Wolf, "Electromagnetic diffraction in optical systems. II. Structure of the image field in an aplanatic system," *Proc. R. Soc. London Ser. A* **253**(1274), 358–379 (1959).
31. B. T. Draine, "The discrete-dipole approximation and its application to interstellar graphite grains," *Astrophys. J.* **333**, 848–872 (1988).
32. L. Novotny and B. Hecht, *Principles of Nano-Optics*, Cambridge University Press, Cambridge, UK (2007).
33. T. Iida and H. Ishihara, "Theoretical study of the optical manipulation of semiconductor nanoparticles under an excitonic resonance condition," *Phys. Rev. Lett.* **90**(5), 057403 (2003).
34. R. Bresolí-Obach et al., "Chemical control over optical trapping force at an interface," *Adv. Opt. Mater.* **10**, 2200940 (2022).
35. J. R. Arias-González and M. Nieto-Vesperinas, "Optical forces on small particles: attractive and repulsive nature and plasmon-resonance conditions," *J. Opt. Soc. Am. A* **20**(7), 1201–1209 (2003).
36. S. Albaladejo et al., "Scattering forces from the curl of the spin angular momentum of a light field," *Phys. Rev. Lett.* **102**(11), 113602 (2009).
37. T. Kudo, S. J Yang, and H. Masuhara, "A single large assembly with dynamically fluctuating swarms of gold nanoparticles formed by trapping laser," *Nano Lett.* **18**(9), 5846–5853 (2018).
38. L. Paterson et al., "Controlled rotation of optically trapped microscopic particles," *Science* **292**(5518), 912–914 (2001).
39. M. Padgett and R. Bowman, "Tweezers with a twist," *Nat. Photonics* **5**, 343–348 (2011).
40. A. Bishop et al., "Optical microrheology using rotating laser-trapped particles," *Phys. Rev. Lett.* **92**,198104 (2004).
41. Y. Arita, M. Mazilu, and K. Dholakia, "Laser-induced rotation and cooling of a trapped microgyroscope in vacuum," *Nat. Commun.* **4**, 2374 (2013).
42. J. Ahn et al., "Ultrasensitive torque detection with an optically levitated nanorotor," *Nat. Nanotechnol.* **15**, 89–93 (2020).
43. R. Paschotta, *Field Guide to Laser Pulse Generation*, SPIE Press (2008).
44. A. Maheshwari and A. De, "Theoretical investigation on nonlinear optical effects in laser trapping of dielectric nanoparticles with ultrafast pulsed excitation," *Opt. Express* **24**(19), 21485–21496 (2016).
45. R. W. Boyd, *Nonlinear Optics*, Academic Press (2020).
46. A. C. Durand et al., "Force and torque on an electric dipole by spinning light fields," *Phys. Rev. A* **88**(3), 033831 (2013).
47. Y. Huang et al., "Tunable lattice coupling of multipole plasmon modes and near-field enhancement in closely spaced gold nanorod arrays," *Sci. Rep.* **6**(1), 23159 (2016).
48. T. Schumacher et al., "Nanoantenna-enhanced ultrafast nonlinear spectroscopy of a single gold nanoparticle," *Nat. Commun.* **2**, 333 (2011).
49. T. Cesca et al., "Local-field enhancement effect on the nonlinear optical response of gold-silver nanoplanets," *Opt. Express* **20**(4), 4537–4547 (2012).
50. R. K. Harrison and A. B. Yakar, "Role of near-field enhancement in plasmonic laser nanoablation using gold nanorods on a silicon substrate," *Opt. Express* **18**(21), 22556–22571 (2010).
51. D. J. Wu and X. J. Liu, "Optimization of silica–silver–gold layered nanoshell for large near-field enhancement," *Appl. Phys. Lett.* **96**(15), 151912 (2010).
52. R. R. Anderson and J. A. Parrish, "Selective photothermolysis: precise microsurgery by selective absorption of pulsed radiation," *Science* **220**(4596), 524–527 (1983).
53. K. M. McPeak et al., "Plasmonic films can easily be better: rules and recipes," *ACS Photonics* **2**, 326–333 (2015)
54. M. Daimon and A. Masumura, "Measurement of the refractive index of distilled water from the near-infrared region to the ultraviolet region," *Appl. Opt.* **46**, 3811–3820 (2007).
55. W. Huang et al., "Effect of the lattice crystallinity on the electron−phonon relaxation rates in gold nanoparticles," *J. Phys. Chem. C* **111**, 10751–10757 (2007).
56. M. Hu and G. V. Hartland, "Heat dissipation for Au particles in aqueous solution: relaxation time versus size," *J. Phys. Chem. B* **106**(28), 7029–7033 (2002).
57. G. Baffou and H. Rigneault, "Femtosecond-pulsed optical heating of gold nanoparticles," *Phys. Rev. B* **84**(3), 035415 (2011).
58. G. Baffou and R. Quidant, "Thermo-plasmonics: using metallic nanostructures as nano-sources of heat," *Laser Photonics Rev.* **7**(2), 171–187 (2013).
59. A. J. Schmidt et al., "Thermal conductance of hydrophilic and hydrophobic interfaces," *J. Phys. Chem. C* **112**, 13320–13323 (2008).
60. Z. Ge, D. G. Cahill, and P. V. Braun, "Thermal conductance of hydrophilic and hydrophobic interfaces," *Phys. Rev. Lett.* **96**, 186101 (2006).

Zheng Zhu is a PhD candidate at the optics research group, Delft University of Technology. He joined the joint training program of the Delft University of Technology and Shenzhen University. He is now under the supervision of Prof. Paul Urbach and Prof. Xiaocong Yuan. His research interests include nonlinear optical trapping, localized surface plasmons, and ultrafast optics. He now works as a research assistant at the Zhejiang lab.

Yuquan Zhang received his PhD in optical engineering from Nankai University, China, in 2015. Currently, he is an associate professor in the Nanophotonics Research Center of Shenzhen University. His research interests include singular optical field modulation, optical tweezers, surface/tip-enhanced Raman spectroscopy, and superresolution imaging. Recently, his research has focused on plasmonic trapping and nonlinear effects in optical traps.

Shuoshuo Zhang is a PhD candidate in Nanophotonics Research Center of Shenzhen University. He received his master's degree in optical engineering from Shandong University of Technology, China, in 2020. His research interests include spatiotemporally structured light, ultrafast optics, and nonlinear optical tweezers.

Aurèle J. L. Adam is an assistant professor at Delft University of Technology. He joined the research team of Alain Kreisler at the Laboratoire de Génie Électrique de Paris (University Paris VI – CNRS) and the microelectronics group of Erik Kollberg at the Chalmers University of Technology (Sweden) for a coupled PhD thesis. The core of his research is the study of feasibility and utility of near-field techniques at terahertz frequencies.

Changjun Min received his BS and PhD degrees from the University of Science and Technology of China, followed by postdoctoral positions at Louisiana State University, and then Nanyang Technological University. In 2014, he joined the Nanophotonics Research Center in Shenzhen University as a professor. His research interests include plasmonics, optical tweezers, vector beams, surface-enhanced Raman scattering, and metasurfaces.

Hendrik Paul Urbach is a professor at Delft University of Technology. He joined Philips Research Laboratory in Eindhoven ("Nat.Lab" as it was known at the time), where he was appointed Principal Scientist. In 2000, he became part-time professor of diffraction optics at Delft University of Technology. In 2008, he became group leader of the Optics Research Group of Delft University of Technology. His research interests include direct and inverse problems of high-resolution optical imaging, diffraction theory, and the application of asymptotic methods to optics.

Xiaocong Yuan is Changjiang Scholar Professor and director of the Nanophotonics Research Center in Shenzhen University. He received his PhD in physics from King's College London in 1994. He is now a fellow of SPIE and Optica, and a board member of the Chinese Optical Society and the Chinese Optical Engineering Society. His research interests include singular optics, nanophotonics, plasmonics, advanced light manipulations, and their applications in communications, imaging, and optical tweezers.